Manuscript prepared for Biogeosciences Discuss.
with version 2015/04/24 7.83 Copernicus papers of the LaTeX class copernicus.cls.
Date: 19 February 2016

Uncertainty analysis of gross primary production partitioned from net ecosystem exchange measurements

R. Raj, N. A. S. Hamm, C. van der Tol, and A. Stein

Faculty of Geo-Information Science and Earth Observation (ITC), University of Twente, PO Box 217, 7514 AE Enschede, the Netherlands

Correspondence to: R. Raj (r.raj@utwente.nl)

Abstract

Gross primary production (GPP) can be separated from flux tower measurements of net ecosystem exchange (NEE) of CO_2. This is used increasingly to validate process-based simulators and remote sensing-derived estimates of simulated GPP at various time steps. Proper validation includes the uncertainty associated with this separation. In this study, uncertainty assessment was done in a Bayesian framework. It was applied to data from the Speulderbos forest site, The Netherlands. We estimated the uncertainty in GPP at half hourly time steps, using a non-rectangular hyperbola (NRH) model for its separation from the flux tower measurements. The NRH model provides a robust empirical relationship between radiation and GPP. It includes the degree of curvature of the light response curve, radiation and temperature. Parameters of the NRH model were fitted to the measured NEE data for every 10-day period during the growing season (April to October) in 2009. We defined the prior distribution of each NRH parameter and used Markov chain Monte Carlo (MCMC) simulation to estimate the uncertainty in the separated GPP from the posterior distribution at half-hourly time steps. This time series also allowed us to estimate the uncertainty at daily time steps. We compared the informative with the non-informative prior distributions of the NRH parameters and found that both choices produced similar posterior distributions of GPP. This will provide relevant and important information for the validation of process-based simulators in the future. Furthermore, the obtained posterior distributions of NEE and the NRH parameters are of interest for a range of applications.

1 Introduction

Net ecosystem exchange (NEE) is a terrestrial component of the global carbon cycle. It is the exchange of CO_2 between the terrestrial ecosystem and the atmosphere. The measurement of NEE by the eddy covariance technique is well-established (Baldocchi, 2003). Specifically, NEE is the balance between the CO_2 released by the ecosystem respiration (R_{eco}) and the gross CO_2 assimilated via photosynthesis. The fraction of carbon in the assimilated CO_2 is the gross primary production (GPP). Estimates of GPP provide information about the physiological processes that contribute to NEE (Aubinet et al., 2012). Measured NEE data are used to validate the NEE that is simulated by ecosystem process-based simulators such as BIOME-BGC (BioGeochemical Cycles) (Thornton, 1998). It is often desirable to validate the simulated component flux (R_{eco} and GPP) independently. This is particularly important for diagnosing the misrepresentation (overestimation or underestimation) of assimilation processes in the simulator (Reichstein et al., 2005), which can only be achieved by comparing the GPP partitioned from NEE data with the simulated one. Furthermore, remote sensing-derived light use efficiency (LUE) models address the spatial and temporal dynamics of GPP (Running et al., 2004). The reliability of such models at the regional scale relies on the validation using GPP partitioned from NEE data (Wang et al., 2010; Li et al., 2013).

Flux partitioning methods (FPM) are used to partition NEE into its component flux (GPP and R_{eco}). These methods are based on fitting a non-linear empirical model to the measured NEE data and other meteorological data in order to estimate the parameters. The estimated parameters of the non-linear model are then used to predict daytime R_{eco} and GPP. There are two types of FPM: (1) those that use only nighttime NEE data, and (2) those that use either daytime NEE data or both daytime and nighttime data (Lasslop et al., 2010; Stoy et al., 2006; Aubinet et al., 2012).

A nighttime-based FPM assumes that NEE is equal to R_{eco} (GPP $= 0$ during the night) and that it varies with air and soil temperature (Richardson et al., 2006a). A daytime-based FPM assumes that the variation of NEE occurs with photosynthetic photon flux density

(PPFD) and the light response curve (plot of NEE against PPFD) can be represented by a rectangular hyperbola (RH) model (Ruimy et al., 1995). Lasslop et al. (2010) proposed a daytime-based FPM using the RH model by incorporating the variation of NEE as a function of global radiation, air temperature, and vapour pressure deficit (VPD) because these affect GPP via stomatal regulation. A daytime-based FPM was proposed that uses the non-rectangular hyperbola (NRH) model to incorporate the effect of the degree of curvature (θ) of the light response curve (Gilmanov et al., 2003; Rabinowitch , 1951). θ represents the convexity of the light response curve as the NEE and radiation relationship approaches saturation. Further, the light response curve represented by the NRH model has been found to fit NEE data better than the RH model (Gilmanov et al., 2003; Aubinet et al., 2012). Gilmanov et al. (2013) further improved the NRH model by incorporating the effect of VPD and temperature as proposed by Lasslop et al. (2010). They used PPFD and soil temperature instead of global radiation and air temperature respectively. This improvement incorporates the influence of PPFD, air or soil temperature, VPD, and θ by taking advantage of better representation of the light response curve by comparison to the RH model.

A quantification of uncertainty in partitioned GPP provides an associated credible interval that can be used for proper implementation of calibration and validation of a process-based simulator against partitioned GPP (Hagen et al., 2006). The temporal resolution of process-based simulators may vary from half-hourly to monthly. It is therefore necessary to quantify uncertainty associated with the partitioned GPP at half-hourly to monthly time scales. For example, the partitioned GPP and associated uncertainty at a daily time scale can provide data for the calibration of process-based simulators such as BIOME-BGC.

In this study, we adopted the NRH model to partition half-hourly GPP from NEE data. In the past, numerical optimization has been used to estimate a single optimized value of each model parameters (Gilmanov et al., 2003, 2013). This did not quantify the uncertainty in half-hourly partitioned GPP. The measurements of half-hourly NEE are uncertain. Therefore, the optimized parameters are also uncertain (Richardson and Hollinger, 2005). Obtaining the underlying probability distribution of the NRH parameters gives a measure of uncertainty in parameters, which can be further propagated towards the NRH model to

estimate uncertainty in partitioned GPP. A Bayesian implementation provides a solution to quantify the uncertainty in model parameters in the form of probability distributions (Gelman et al., 2013). The Bayesian approach was used in other studies to constrain the parameters of process-based simulators by using either eddy covariance data, biometric data, or both (Du et al., 2015; Minet et al., 2015; Ricciuto et al., 2008). We applied the Bayesian approach to a different type of model. We fitted the non-linear empirical NRH model to NEE data and quantified the uncertainty in NRH parameters to partition GPP with uncertainty.

The objective of this study was to implement a Bayesian approach for quantification of the uncertainty in half-hourly partitioned GPP using the NRH model given the availability of half-hourly NEE and other meteorological data. The time series of empirical distributions of half-hourly GPP values also allowed us to estimate the uncertainty in GPP at daily time steps. Data were available from a flux tower in the central Netherlands at the Speulderbos forest. This will provide relevant and important information for the validation of process-based simulators.

2 Methods

2.1 Study area and data

The Speulderbos forest is located at $52^{\circ}15'08''$ N, $5^{\circ}41'25''$ E within a large forested area in the Netherlands. There is a flux tower within a dense 2.5 ha Douglas fir stand. The stand was planted in 1962. The vegetation, soil, and climate of this site have been thoroughly described elsewhere (Steingrover and Jans, 1994; Su et al., 2009; van Wijk et al., 2001).

The CSAT3, Campbell Sci, LI7500 LiCor Inc, and CR5000 instruments were installed in June 2006 and have been maintained, and the data processed (software AltEddy, Alterra) by C. van der Tol (University of Twente, co-author) and A. Frumau (Energy Centre Netherlands). We examined half-hourly NEE data (measured at the flux tower) for the growing season (April to October) of 2009. The quality of the NEE data were assessed using the Foken classification system, which provides a flag to each half-hourly NEE datum from 1

through 9 (Foken et al., 2005). Each flag is associated with: (a) the range of the steady state condition of the covariance of vertical wind speed and CO_2 concentration of half-hour duration, (b) the range of the integral turbulence characteristic parameter indicating the developed turbulence; and (c) the range of the orientation of the sonic anemometer to make sure that the probe is omnidirectional at the time of measurements. We followed the suggestion of Foken et al. (2005) and accepted only those NEE data that were labelled from 1 to 3. For the growing season, we acquired half-hourly PPFD from the sensor PARlite (Kipp & Zonen. Delft, the Netherlands) and half-hourly T_a from the weather sensor WXT510 (Vaisala, Finland) installed at the flux tower.

2.2 The non-rectangular hyperbola (NRH) model

NEE is given as:

$$\mathrm{NEE} = P_a - R_{eco} \tag{1}$$

where NEE is measured by the eddy covariance technique and P_a is gross CO_2 assimilation. The exchange of carbon into the system through photosynthesis is considered a positive flux because it represents production and the loss of carbon through respiration is considered a negative flux.

The light response curve is represented using the NRH model (Gilmanov et al., 2003; Rabinowitch , 1951):

$$P_a = \frac{1}{2\theta} \times \left(\alpha \cdot \mathrm{PPFD} + A_{max} - \sqrt{(\alpha \cdot \mathrm{PPFD} + A_{max})^2 - 4\alpha \cdot A_{max} \cdot \theta \cdot \mathrm{PPFD}} \right) \tag{2}$$

where α is the apparent quantum yield, A_{max} is the photosynthetic capacity at light saturation, and θ is the degree of curvature of the light response curve.

Gilmanov et al. (2013) modelled ecosystem respiration R_{eco} using the temperature dependent term according to Van't-Hoff's equation in its exponential form (Thornley and Johnson, 2000):

$$R_{eco} = r_0 \times \exp(k_T T_a) \tag{3}$$

where T_a is the air temperature and r_0 and k_T are the temperature sensitivity coefficients. Eqs. 2 and 3 are substituted in Eq. (1) to obtain the model for net ecosystem exchange NEE:

$$\mathrm{NEE} = \frac{1}{2\theta} \times \left(\alpha \cdot \mathrm{PPFD} + A_{max} - \sqrt{(\alpha \cdot \mathrm{PPFD} + A_{max})^2 - 4\alpha \cdot A_{max} \cdot \theta \cdot \mathrm{PPFD}} \right) - r_0 \times \exp(k_T T_a). \quad (4)$$

Both daytime and nighttime half-hourly NEE, PPFD, and T_a data were used to estimate the NRH model parameters $\boldsymbol{\beta}$ = (θ, α, A_{max}, r_0, k_T) (Eq. 4). For nighttime data, Eq. (4) includes only the respiration term because PPFD is equal to zero during the night. These estimated parameters, together with half-hourly PPFD, were used in Eq. (2) to calculate half-hourly P_a. Values of half-hourly GPP were calculated by multiplying P_a by 12/44 (12 is the atomic mass of carbon, and 44 is the atomic mass of CO_2) in order to convert the mass of CO_2 into the mass of carbon (C). This gives GPP in mg C $m^{-2}\,s^{-1}$. This unit is the same as the unit of GPP simulated by process-based simulators such as BIOME-BGC. Therefore, the simulated GPP could be directly compared to the partitioned GPP in the future at the study area. The unit of P_a is the same as the unit of measured NEE in mg $CO_2\,m^{-2}\,s^{-1}$. The unit of each parameter and other variables used in the above equations are shown in Table 1. Gilmanov et al. (2013) proposed to incorporate the effect of VPD by multiplying Eq. (2) by the VPD-response function, ϕ, that accounts for the VPD limitation on P_a. The function ϕ is set equal to 1 if VPD is below some critical value (VPD_{cr}) that indicates that water stress does not affect photosynthesis. Above the critical value ($VPD > VPD_{cr}$), ϕ decreases exponentially with the curvature parameter σ_{VPD}, which may vary between 1 and 30 kPa. Low values of σ_{VPD} indicate a strong water stress effect, whereas higher values indicate a weak water stress effect. We calculated half-hourly VPD from relative humidity (RH) using the procedure provided in Monteith and Unsworth (1990). We found that 90 % of the total half-hourly VPD values in the growing season of 2009 were less than 1 kPa and 9 % were between 1 kPa and 1.5 kPa. We therefore neglected the influence of VPD as

a limiting factor for the water stress at Speulderbos. This follows Körner (1995) and Lasslop et al. (2010) who specified $\text{VPD}_{\text{cr}} = 1$. We, therefore, assumed ϕ equal to 1.

2.3 Theory of Bayesian inference for the model parameters

Bayesian inference treats all parameters as random variables (Gelman et al., 2013). Bayes rule is given as

$$p(\boldsymbol{\beta}|\mathbf{y}) = \frac{p(\mathbf{y}|\boldsymbol{\beta})p(\boldsymbol{\beta})}{p(\mathbf{y})} \propto \text{likelihood} \times \text{prior} \tag{5}$$

where $p(\boldsymbol{\beta})$ is the prior distribution, representing the prior understanding of uncertainty in the model parameters values before the observations are taken into account. This understanding may come from expert judgement or previously published research on the parameters (Oakley and O'Hagan, 2007; Raj et al., 2014). If no prior knowledge is available, non-informative priors may be used (i.e., a wide prior distribution that conveys no prior information). The term $p(\boldsymbol{\beta}|\mathbf{y})$ is the posterior distribution of $\boldsymbol{\beta}$ after combining prior knowledge and data $\mathbf{y}$ and represents the uncertainty in $\boldsymbol{\beta}$ given the data and the prior. The marginal effect of each parameter $p(\beta_i|\mathbf{y}), i = 1, 2, \ldots, n$, is the main quantity of interest, expressing the uncertainty in each parameter separately. The term $p(\mathbf{y}|\boldsymbol{\beta})$ is the conditional probability of observing data $\mathbf{y}$ given $\boldsymbol{\beta}$ and is also called the likelihood. The term $p(\mathbf{y})$ is the probability of observing the data $\mathbf{y}$ before observations were taken. This acts as the normalising constant that ensures that $p(\boldsymbol{\beta}|\mathbf{y})$ is a valid probability distribution that integrates to 1. For most real-world problems it is not possible to write down analytical solutions for Eq. (5) and it is usual to perform inference using Markov Chain Monte Carlo (MCMC) simulation (Gelman et al., 2013).

MCMC is a method for conducting inference on $p(\boldsymbol{\beta}|\mathbf{y})$. It requires evaluation of the joint distribution $p(\mathbf{y}|\boldsymbol{\beta})p(\boldsymbol{\beta})$, which represents the dependence structure in the data. MCMC constructs Markov chains of the parameters space and generates samples $\boldsymbol{\beta}^{(1)}$, $\boldsymbol{\beta}^{(2)}, \ldots, \boldsymbol{\beta}^{(m)}$ of $\boldsymbol{\beta}$ whose unique stationary distribution is the posterior distribution of interest $p(\boldsymbol{\beta}|\mathbf{y})$. The m samples are then used to conduct inference on each β_i. For example the

mean, median and 95 % credible interval can all be calculated over these m samples. It is usual to construct multiple Markov chains and to assess whether they converge to the same stationary distribution. We refer the reader to chapter 4 in Lunn et al. (2013) and chapter 11 in Gelman et al. (2013) for further explanation.

2.4 Implementation of Bayesian inference for the NRH model parameters

We treated Eq. (4) as a non-linear regression problem:

$$\begin{aligned} y_i &= \frac{1}{2\theta} \times \left(\alpha \cdot \mathsf{PPFD}_i + A_{\mathsf{max}} - \sqrt{(\alpha \cdot \mathsf{PPFD}_i + A_{\mathsf{max}})^2 - 4\alpha \cdot A_{\mathsf{max}} \cdot \theta \cdot \mathsf{PPFD}_i} \right) \\ &- r_0 \times \exp(k_{\mathsf{T}} T_{\mathsf{a}_i}) + \varepsilon_i \\ &= \mu_i - \nu_i + \varepsilon_i \end{aligned} \tag{6}$$

where y is the response variable (NEE), PPFD and T_{a} are the predictor variables and ε is the residual error. The residual error arose because the model did not perfectly fit the data. The subscript i indicates a single observation. For brevity we use μ_i to refer to the first term on the RHS and ν_i to refer to the second term on the right hand side of Eq. 6.

As is usual in regression modelling, we assumed normally distributed errors, hence $\varepsilon_i \sim N(0, \sigma^2)$ and the likelihood also followed a normal distribution, such that $y_i \sim N(\mu_i - \nu_i, \sigma^2)$. In the above notation, $\boldsymbol{\beta} = (\alpha, A_{\mathsf{max}}, \theta, r_0, k_{\mathsf{T}})^T$ and the likelihood is $p(\mathbf{y}|\boldsymbol{\beta}, \sigma^2)$, where $\mathbf{y} = (y_1, y_2, \ldots, y_n)^T$ for n observations.

In Bayesian analysis it is usual to refer to precision, which is the inverse of the variance, hence $\tau_e = 1/\sigma^2$. Further, the assumption of prior distributions for each β_i together with τ_e is required. No prior information was available for τ_e so a non-informative prior was selected. We assumed a Gamma distribution for τ_e with shape and rate parameters equal to 0.001. This ensures a non-negative non-informative prior for τ_e (Lunn et al., 2013).

We made two choices for the prior distribution for each β_i. First, a non-informative prior was used (Sect. 2.4.1). Second, prior information for each β_i was obtained from the literature, being called an informative prior distribution (Sect. 2.4.2). Note that the same

non-informative prior for τ_e was used in both choices. The results for informative an non-informative priors were compared.

2.4.1 Non-informative prior distributions

We assumed a normal distribution for each β_i with mean equal to 0 and standard deviation equal to 32, which gives small value of the the precision equal to 0.001 to make the distribution wide. NRH is a non-linear model and therefore appropriate constraints should be imposed to ensure the meaningful values of the prior parameter distribution (Lunn et al., 2013). Each β_i parameter must be positive (Sect. 2.4.2) so we truncated the normal distribution on each β_i except θ to ensure only positive values. For θ, we truncated the normal distribution to occur between 0 and 1 by setting the obvious limit to this parameter (see also item 2 in Sect. 2.4.2). The above choices ensure wide non-informative prior distributions whilst specifically excluding physically unrealistic values.

2.4.2 Informative prior distributions

Below we justify choices for the informative prior distributions on $\boldsymbol{\beta}$.

1. The quantum yield, α, represents the amount of absorbed CO_2 per quanta of absorbed light. Cannell and Thornley (1998) reported that α varies little among C_3 species and has a value from 0.09 to 0.11 and from 0.04 to 0.075 mol CO_2 (mol quanta)$^{-1}$ in saturated and ambient CO_2 conditions respectively. The typical value of α equals 0.05 mol CO_2 (mol quanta)$^{-1}$ for a C_3 species in an ambient atmosphere (Skillman, 2008; Long et al., 2006; Bonan et al., 2002). Douglas fir at Speulderbos is a C_3 species. We used this information to construct the prior distribution on α, as follows:

   – A value of α around 0.05 has the highest probability. The probability decreases as the value of α decreases or increases from 0.05 and cannot be negative. The maximum value that α can attain is 0.11.

– We assumed a normal distribution of α with mean, $\mu_\alpha = 0.05$, and variance, $\sigma_\alpha^2 = (0.015)^2$ (i.e, standard deviation, $\sigma_\alpha = 0.015$). The choice of mean ensures that the highest probability is assigned to the values around 0.05. The choice of variance ensures that 99.7 % ($\mu \pm 3\sigma_\alpha$) of α is positive and lies in the interval between 0 and 0.11. We also truncated 0.3 % of negative α values from the assumed normal distribution. In the unit of mg CO_2 (µmol quanta)$^{-1}$, the assumed normal distribution ($N(\mu_\alpha = 0.05,\ \sigma_\alpha = 0.015)$) is expressed as $N(0.0022, 0.00066)$ (Fig. 1a).

2. The curvature parameter θ can take values from 0, which reduces Eq. (4) to the simpler rectangular hyperbola, to 1, which describes the Blackman response of two intersecting lines (Blackman, 1905). The physiological range for θ has been observed to be between 0.5 and 0.99 (Ogren, 1993; Cannell and Thornley, 1998). A value of $\theta = 0.9$ was recommended by Thornley (2002) and at $\theta = 0.8$ by Johnson et al. (2010) and Johnson (2013). The estimate of θ, as a result of fitting the NRH model to either measured photosynthesis or NEE data was found to be in the range of 0.7 to 0.99 (Gilmanov et al., 2010, 2003). These findings for θ indicated that a higher probability should be assigned to the values around 0.8 and the probability should approach to zero below 0.5. This means that the distribution of θ can be assumed to be negatively skewed with Pr($\theta < 0.5$) approaching zero and Pr($\theta \approx 0.8$) at a maximum. These conditions were modelled using a beta distribution with shape parameters at 10 and 3 for θ (Fig. 1b).

3. The photosynthetic capacity at light saturation A_{max} is reached when the photosynthesis is Rubisco limited and varies among different tree species (Cannell and Thornley, 1998). At the canopy level, A_{max} also depends upon the structure of the canopy (i.e., arrangement of the canopy leaves) and the area of leaves available to absorb photons. Both are determined by the leaf area index (LAI) (Ruimy et al., 1995). We compiled the prior information on A_{max} for Douglas fir species from the literature. Values of A_{max} were mainly reported for needles, whereas the NRH model (Eq. 4)

requires A_{max} values for the canopy. Scaling A_{max} from needle to the canopy equivalent is not a trivial task because this depends on the light distribution and the vertical profile of A_{max} in the canopy. Here we analysed plateau values of photosynthesis at needle and canopy level with simulations by a model that takes this into account: the model SCOPE (van der Tol et al., 2009). These simulations (not shown) indicated that the relation between the two plateaus (canopy : needle A_{max}) increased with LAI but saturated at a value of 2.8. The mean value of LAI at the Speulderbos site is high (approximately 9 van Wijk et al., 2000; Steingrover and Jans, 1994) and therefore we could translate the reported range of A_{max} values for the Speulderbos (Mohren, 1987) of 0.26 to 0.52 mg CO_2 m^{-2} s^{-1} into values of 0.73–1.46 mg CO_2 m^{-2} s^{-1} for canopy A_{max}. van Wijk et al. (2002) reported slightly higher canopy A_{max} values of 1.86 and 1.06 mg CO_2 m^{-2} s^{-1} at the Speulderbos site. The highest and lowest value for needle A_{max} for Douglas fir (irrespective of the site) we found in the literature were 0.097 (canopy $A_{\text{max}} = 0.27$) and 1.01 mg CO_2 m^{-2} s^{-1} (canopy $A_{\text{max}} = 2.8$) respectively (Ripullone et al., 2003; Warren et al., 2003; Lewis et al., 2000). To cover this rather wide range of values, a Gamma distribution with shape and rate parameters equal to 4 and 2.5 respectively was selected to ensure higher probabilities are assigned to the values between 1 and 2.5 with decreasing probabilities down to 0 and up to 4.5 (Fig. 1c). The A_{max} values at Speulderbos are well placed in the overall distribution.

4. The parameters for temperature sensitivity k_{T} and Q_{10} are related as $Q_{10} = \exp(10k_{\text{T}})$ (Davidson et al., 2006). Q_{10} is the factor by which respiration (Eq. 3) is multiplied when temperature increases by 10 °C. (Mahecha et al., 2010) carried out experiments across 60 FLUXNET sites to check the sensitivity of ecosystem respiration to air temperature. They suggested that Q_{10} does not differ among biomes and is confined to values around 1.4 ± 0.1 (corresponding to k_{T} around 0.034 ± 0.008). Hence $k_{\text{T}} \approx 0.034$ should have the highest probability of occurrence. Q_{10} data reported in the supporting material of Mahecha et al. (2010) showed that that Q_{10} becomes less frequent as it increases or decreases from 1.4 and attains a highest value of ~ 2.72

(corresponding to k_T = 0.1). To model these conditions a Gamma prior distribution was chosen with shape and rate parameters equal to 4 and 120 respectively (Fig. 1d).

5. The r_0 parameter represents the ecosystem respiration at 0 °C. We adopted the following steps to define the prior distribution for r_0.

   – Mahecha et al. (2010) presented a graph of seasonal variation of ecosystem respiration at 15 °C (R_b) for 60 FLUXNET sites. We extracted the values of R_b (in g $CO_2\,m^{-2}$ day^{-1}) from the graph for those sites that belong to evergreen needle leaf forest (ENF). We obtained the values of r_0 from R_b using the following equations:

   $$r_0 = \frac{R_b}{\exp(k_T \times 15)} \tag{7}$$

   where k_T was obtained from Q_{10} as reported in point 4 above. Site specific Q_{10} value is used here. The unit of r_0 is converted into mg $CO_2\,m^{-2}\,s^{-1}$.

   – We identified values of r_0 for ENF in the range 0.013 to 0.07 mg $CO_2\,m^{-2}\,s^{-1}$. We also identified values of r_0 in the range 0.019 to 0.043 at the Loobos FLUXNET site in the Netherlands (Mahecha et al., 2010), which is close to Speulderbos. Therefore, we assumed that the most frequent values of r_0 at Speulderbos are in this range. To model these conditions we chose a Beta distribution with shape parameters at 2 and 64 (Fig. 1e).

2.4.3 Bayesian inference of β

We used WinBUGS software version 1.4.3 (Lunn et al., 2000) to implement the Bayesian full probability models (Eq. 5) for the inference of β. WinBUGS is a windows implementation of the original BUGS (Bayesian Inference Using Gibbs Sampling) software. This was a joint initiative between the MRC Biostatistics Unit, Cambridge and the Imperial College School of Medicine, London (Lunn et al., 2013). WinBUGS implements MCMC for Bayesian inference.

The major inputs of WinBUGS are: (a) the model file specifying the definition of the prior distribution of each β_i and likelihood function, (b) the number of Markov chains to create, (c) the number of iterations for MCMC to carry out for each Markov chain, (d) the burn-in period for which the MCMC runs are discarded, (e) initial values of each β_i for each Markov chain. The burn-in period is the number of samples after which the Markov chains converge to a stationary distribution. The post burn-in samples are used to perform inference on the β_i s.

We obtained the posterior distribution of each β_i for every 10-day block (total 22 blocks) in the growing season of 2009. More precisely, we obtained varying parameters and did not assume values to be constant for the whole study period. This approach is recommended by Aubinet et al. (2012), since obtaining varying parameters incorporates indirectly the temporal changes in the factors such as canopy structure, soil moisture and ecosystem nutrient levels that affect GPP. NRH model does not include these factors directly. Hence, although these factors are not included in the NRH model our implementation does account for them. The 10-day block was chosen because it was sufficiently long to ensure a suitably large NEE dataset *within* the 10-day block but was short enough that we could account for temporal changes *between* the 10-day blocks. Thus the temporal change is observed between consecutive blocks, not within a block. The sample size within a 10-day block was limited because $\sim 30\,\%$ of the data were typically discarded as being of low quality (Foken flag 4 or higher, see Sect. 2.1).

We identified the appropriate length of the burn-in for both informative and non-informative prior distributions. We calculated the Gelman–Rubin potential scale reduction factor (PSRF) to evaluate the convergence of Markov chains for each β_i for the post burn-in period. Graphically, we assessed the convergence of Markov chains by plotting them together for each β_i. This plot is known as trace plot. A visual observation of a proper mixing of these chains indicates the convergence of Markov chains to the stationary distribution. An explanation of PSRF and the identification of the length of the burn-in are given in the Supplement. We refer the reader to pages 71–76 in Lunn et al. (2013) and pages 281–285 in Gelman et al. (2013) for further explanation. Based on that analysis we used three

Markov chains with 16 000 and 25 000 iterations for each chain for informative and non-informative prior distributions respectively. We stored the posterior samples of each β_i and τ_e for the remaining 30 000 samples (i.e., 10 000 post burn-in samples for each of three Markov chains). The BUGS code (model file for WinBUGS) is given in the Supplement.

2.5 Posterior prediction

To perform prediction for a given PPFD_0 and T_{a_0}, m post burn-in samples of $\boldsymbol{\beta}$ and σ^2 were used as follows:

$$\mu_0^{(l)} = \frac{1}{2\theta^{(l)}} \times \left(\alpha^{(l)} \cdot \mathrm{PPFD}_0 + A_{\mathrm{max}}^{(l)} - \sqrt{(\alpha^{(l)} \cdot \mathrm{PPFD}_0 + A_{\mathrm{max}}^{(l)})^2 - 4\alpha^{(l)} \cdot A_{\mathrm{max}}^{(l)} \cdot \theta^{(l)} \cdot \mathrm{PPFD}_0} \right)$$

$$\nu_0^{(l)} = r_0^{(l)} \times \exp\left(k_T^{(l)} T_{a_0}\right)$$

$$y_0^{(l)} \sim N(\mu_0^{(l)} - \nu_0^{(l)}, \sigma^{2(l)}) \quad (8)$$

where (l) is not an exponent, but indicates a specific sample. Other terms are as defined for Eq. (6). The m samples were used to build up the posterior predictive distribution. In this way posterior predictions of GPP (μ_0) and NEE (y_0) were obtained. Note that the uncertainty in the posterior predictions of GPP arose due to uncertainty in the posterior estimates of $\boldsymbol{\beta}$. Uncertainty in the posterior prediction of NEE also considered the uncertainty arising due to the residual error.

Prediction was performed for each 10-day sample for $m = 30\,000$ samples (3 chains and 10 000 samples per chain). These were then summarized (median and 95 % credible interval) to obtain the posterior predictive inference for NEE and GPP for each 10-day block. These 95 % credible intervals show the uncertainty. Hence the actual values of NEE and GPP are likely to be in this interval, but not necessarily at the median. We reported the number of half-hourly NEE measurements that lie inside and outside of 95 % credible intervals of the corresponding half-hourly modelled NEE distributions. In this way, we checked whether realistic credible intervals were obtained. Validation against a separate or hold-out dataset was in principle possible, but was not necessary in this study, because we did not

use the NRH model to predict at blocks outside the range of the data. Moreover, we did not use the posterior $\boldsymbol{\beta}$ values outside the blocks where they were fitted.

3 Results and discussion

3.1 Performance of MCMC

We examined the trace plots of the three Markov chains for each β_i and τ_e obtained for each 10-day block for both choices of informative and non-informative prior distributions. Trace plots for one 10-day block (1 May to 10 May 2009) are shown in Fig. S3 in the Supplement. We observed a proper mixing of the three Markov chains, indicating the convergence of three Markov chains to a stationary distribution that could be used for inference. The Gelman–Rubin PSRF was close to 1 (Table S1 in the Supplement) for each β_i and τ_e, providing further support for the convergence of the Markov chains. The post burn-in samples were used for inference for each 10-day block in the growing season of 2009.

Figure 2 shows the posterior prediction of half-hourly NEE for a 10-day block (1 May to 10 May 2009) for the choice of informative and non-informative prior distributions. The half-hourly NEE was summarized by the median and the 2.5 and 97.5 % iles (i.e., 95 % credible intervals). Out of 338 available half-hourly NEE measurements in this 10-day block, 6 % laid outside the 95 % credible intervals for both choices of prior distribution. This showed that the coverage of the 95 % credible interval was appropriate. There was no substantial difference in the shape of the percentiles curve between the choices of prior distribution. This indicated that the choice of informative or non-informative priors did not influence the posterior prediction of NEE. Similar results were observed for other 10-day blocks. Over the entire 2009 growing season 94 % of the 7126 available half-hourly NEE measurements were bracketed by the 95 % credible intervals for posterior predicted NEE. The choice of informative or non-informative priors did not lead to any substantial difference in the posterior predicted median or 95 % credible intervals.

The 10-day block shown in Fig. 2 shows that the posterior predicted median of NEE was positive during the day and negative during the night. This is to be expected owing to the lack of photosynthesis at night. However, at night the 95 % credible interval spanned zero implying that, when prediction uncertainty is considered, the actual predicted NEE *might* be positive. This is not possible physically, but is an artefact of the statistical approach. Since this is a non-linear regression-type problem the uncertainty in the prediction arises due to both the uncertainty in the estimated regression parameters, $\boldsymbol{\beta}$ and the residual uncertainty. This residual uncertainty was assumed to follow a normal distribution with zero mean and precision, τ_e, and reflects the scatter of the observations round the posterior median prediction. Following our discussion above, this correctly represents the uncertainty in prediction. A consequence of this was that that the prediction intervals were wide and the predictions were potentially positive during the night. This could potentially be addressed by introducing further constraints into the model to allow τ_e to vary temporally (e.g., Hamm et al., 2012). We leave that as a topic for future research whilst noting that our dataset is not very large and we have already fitted a complicated model.

3.2 Uncertainty in partitioned GPP at half-hourly and daily time step

Figure 3 shows the histograms of the posterior distribution of half-hourly and daily-summed GPP for Julian days 121 (1 May) and 196 (15 July) for the choice of both informative and non-informative prior distributions. These allow visualization of the uncertainty within a day and between days for late spring and mid-summer. Clearly the predictions resulting from informative and non-informative priors were similar. For both days higher values of GPP were observed in the afternoon compared to the morning on both Julian days. This reflected the increase in GPP predictions with increasing PPFD from morning to afternoon. The assimilation of carbon was also expected to increase from the start of the growing season to the peak (summer time) of the growing season. It was clear that higher values in GPP were predicted on Julian day 196 compared to Julian day 121 for both morning and afternoon. Seasonal variation in daily GPP was also observed in the daily sum of GPP, which increased from 7–9 $\mathrm{g\,C\,m^{-2}\,d^{-1}}$ on Julian day 121 to 10.5–12.5 $\mathrm{g\,C\,m^{-2}\,d^{-1}}$ on Julian day

196. Variation in daily GPP during the 2009 growing season for the choice of informative priors is shown in Fig 4. The same plot for the choice of non-informative priors is shown in Fig. S4.

We tested whether within the posterior half-hourly GPP distributions, the non-rectangular hyperbolic relationship of GPP with PPFD had been preserved. Figure 5 shows, for an example 10-day block (Julian days 121–130), posterior GPP versus PPDF. The resulting curve shows that the non-rectangular hyperbolic relationship was indeed preserved, and GPP values initially rose and reached a plateau with increasing PPFD. This is important since our daily GPP estimates were obtained by summing half-hourly values. Since the range of PPDF values during the day is large and the relationship between PPFD and GPP non-linear, a realistic representation of the light response curve of GPP is important.

We concluded that the posterior predictions of half-hourly and daily GPP were reliable. We used the posterior distribution of the NRH parameters to predict half-hourly NEE and the 95 % credible intervals bracketed 94 % of the available half-hourly NEE measurements (Sect. 3.1 and Fig. 2). This indicated that our posterior predictions accurately captured the uncertainty in the measured NEE values. We used the same posterior distributions of the NRH parameters to estimate uncertainty in half-hourly GPP. Therefore, we expect that the underlying uncertainty in half-hourly GPP was also accurate.

3.3 Posterior distributions of β

Figure 6 and 7 show the temporal profile (mean and 95 % credible interval) for β for each 10-day block for informative and non-informative prior β distributions respectively.

A clear seasonal pattern in the posterior distribution of α and A_{max} was observed. When using non-informative priors, spikes in the 97.5 % iles for A_{max} were observed at 41, 47, and 59 $\mathrm{mg\,CO_2\,m^{-2}\,s^{-1}}$ (Fig. 7e) for three 10-day blocks (Julian days 91–100, 281–290, and 291–300). These values are physically unrealistic (see Sect. 2.4.2). When using informative priors, the same three 10-day blocks also showed spikes in the 97.5 % iles for A_{max} (Fig. 6e); however these spikes were much smaller and were physically realistic. For other 10-day blocks, both choices of prior yielded comparable posterior distributions of A_{max}

(Figs. 6e and 7f) with uncertainty less than that of the informative and non-informative prior distributions (Fig. 1c and Sect. 2.4.1). The posterior distributions of α, r_0, and k_T were similar for both choices of prior distribution. The choice of non-informative prior yielded wider credible intervals for θ compared to the choice of informative priors (Figs. 6b and 7b).

We calculated the sum of daily GPP for each of the above mentioned 10-day blocks (91–100, 281–290, and 291–300) for both choices of prior (Fig. S5). We found no significant difference in the range of GPP for each block. For example, the range of daily-summed values for 10-day block 281–290 was 26–38 $\mathrm{g\,C\,m^{-2}\,d^{-1}}$ for both choices of prior. This indicated that the unrealistic spikes in the posterior distributions of A_{max} did not affect the prediction of GPP. This led us to evaluate the sensitivity of GPP to A_{max}. We fixed the value of the NRH parameters α, θ, r_0, and k_T at their mean. We varied A_{max} from 0 to 100 $\mathrm{mg\,CO_2\,m^{-2}\,s^{-1}}$ at an interval of 0.5. We estimated the value of GPP at each interval using Eq. 2. A_{max} was varied from 0 to 100 $\mathrm{mg\,CO_2\,m^{-2}\,s^{-1}}$ so that it could cover the spikes in the posterior distributions of A_{max} (Fig. 7e).

The plot of A_{max} against GPP (Fig. 8) revealed that GPP varied strongly up to $A_{\mathrm{max}} = 5\,\mathrm{mg\,CO_2\,m^{-2}\,s^{-1}}$. After this value GPP saturated. The underlying reason is the fact that in light limited conditions, i.e., $A_{\mathrm{max}} \gg \alpha \times \mathrm{PPFD}$, Eq. (2) reduces to $P_a = \alpha \times$ PPFD and hence P_a and thus GPP becomes independent of A_{max}. This explains why the GPP posterior predictions were not affected by the unrealistic values of A_{max} occurring in periods of low light intensities. The choice of prior distribution therefore played a minimal role in the prediction of GPP. The use of informative priors, however, constrained the estimation of the posterior distributions of the parameters.

3.4 Some issues and limitations of this study in estimating uncertainty using the NRH model

The Bayesian approach applied to the NRH model is a solid method to quantify the model parameters and their uncertainty. The 10-day block although suited for the purpose of this study, is insufficient to incorporate the effects of more rapid changes (day to day) in soil moisture and nutrient levels in the NRH model. In principle, these rapid changes could be

incorporated by daily estimation of the NRH parameters (Aubinet et al., 2012; Gilmanov et al., 2013), although this could not be achieved in this study due to the lack of continuous high quality, half-hourly NEE data. The temporal variation in soil moisture and nutrient level for the study site should be investigated further. This may help to select an optimum block size where the within-block variation is limited. The availability of continuous high quality NEE data, however, may impose further constraints on the selection of an optimum block size.

The residual term ε_i in Eq (6) contains the model representation error and the random measurement error. We were unable to separate ε_i into these two components. It is possible to calculate the random measurement error using the paired-measurement approach (Richardson et al., 2006b). Richardson et al. (2008) compared the random measurement error in NEE to ε_i, and concluded that ε_i is mainly due to the random measurement error. We assumed the same to hold for our study, although we could not evaluate this using the paired-measurement approach. Model representation errors included, for example, the fact that we have not parameterized respiration separately for day and night, or separately for vegetation and soil. Vegetation respiration depends also upon other factors, such as irradiance (Sun et al., 2015), photorespiration (because it is nearly proportional to GPP) and produced CO_2 that remains in the trees (Teskey et al., 2008). It is not feasible to model all these processes separately. Thus our model can be expected to contain some representation errors.

Systematic errors also result in uncertainty in NEE measurements (Moncrieff et al., 1996; Aubinet et al., 2012). We have applied the Foken classification system (Sect. 2.1) to filter out the low quality NEE measurements that contain high systematic errors. This reduced the effect of systematic errors on the posterior prediction of NRH parameters and on the model residuals. A source of systematic error that we could not account for was storage of CO_2 below the measurement height during stable conditions at night (Goulden et al., 1996). The turbulent mixing after sunrise may cause hysteresis in the light response curve between morning and late afternoon hours. This hysteresis will contribute to the scatter in the model fit, and thus to the uncertainty in the estimated parameters.

The implementation of the NRH model assumed that PPFD and T_a were known without error and all uncertainty was attributed to the response variable (NEE). This assumption is usual in statistical regression modelling, but is unlikely to be correct in this case. There is scope to incorporate information about uncertainty in PPFD and T_a, although this would lead to a more complicated model. Future research could examine whether relaxing this assumption would improve the model.

We focused in the growing season in 2009. This short period was chosen to illustrate the implementation of the Bayesian approach to quantify the uncertainty in half-hourly partitioned GPP using the NRH model. The study could be extended towards multiple years, allowing a multi-year comparison although that was outside the scope of our methodological focus. Further, different models have been investigated previously to partition GPP (Desai et al., 2008; Richardson et al., 2006a). Any model is a source of uncertainty in itself because it cannot account for every process. The scope of this study can therefore be further widened by addressing multiple established ways of partitioning GPP and thus analysing uncertainty associated with these.

Beer et al. (2010) partitioned GPP from NEE both using the rectangular hyperbola (RH) light-response curve (Lasslop et al., 2010) and a conventional night-time data based approach (Reichstein et al., 2005) for many FLUXNET sites, and further used the partitioned GPP to calibrate five highly diverse diagnostic models for GPP to produce the distribution of global GPP. Although the present study focused on better understanding the uncertainty in partitioning GPP using NRH light-response curve, future research can build on our findings and extend our approach to other sites and years.

4 Conclusions

The study concluded that the choice of informative and non-informative prior distributions of the NRH model parameters led to similar posterior distributions for both GPP and NEE. Obtaining informative priors is time consuming because the values of each parameter are not explicitly mentioned in the literature. Informative priors also require the acquisition of infor-

mation on species or site specific values of photosynthetic capacity at light saturation (A_{max}) and ecosystem respiration at reference temperature (r_0) parameter. As an alternative, non-informative priors can be obtained with proper constraints using minimum information on the NRH parameters such as the positivity of A_{max}. Therefore, non-informative priors can be used for any species type irrespective of study sites. These findings are valuable to conduct uncertainty analysis across a larger sample of sites with different GPP characteristics, e.g., by obtaining NEE and other meteorological data from the FLUXNET data base. The downside of non-informative prior is the production of spikes in the posterior of A_{max} for some days in this study. Therefore, if such values are of interest in a particular study (e.g., photosynthesis nitrogen use efficiency that relies on the ratio of A_{max} and leaf nitrogen) then informative prior should be used.

The estimates of the NRH model parameters were obtained for 10-day blocks. The values of the posterior parameters and their variation over time could provide further understanding of how the forest responds to factors not included in the model, such as soil moisture, nutrition or tree age.

Quantifying uncertainty estimates as empirical distributions in half-hourly gross primary production (GPP) was implemented in the Bayesian framework using the non-rectangular hyperbola (NRH) model. These uncertainty estimates were provided at daily time steps. The approach could be extended to include the uncertainty in meteorological forcing, in particular photosynthetic photon flux density and air temperature. The distributions in half-hourly GPP can be further used to obtain distributions at any desired time steps, such as 8-day and monthly. The uncertainty in GPP estimated in this study can be used further to quantify the propagated uncertainty in the validation of satellite GPP products such as MODIS 17 or process-based simulators such as BIOME-BGC. Although we focussed on quantifying the uncertainty in GPP partitioning, our approach could also be used to either estimate R_{eco} or fill missing NEE data and this will be achieved in the future study.

The Supplement related to this article is available online at doi:10.5194/bgd-0-1-2016-supplement.

Acknowledgements. The authors thankfully acknowledge the support of the Erasmus Mundus mobility grant and the University of Twente for funding this research.

References

Aubinet, M., Vesala, T., and Papale, D.: Eddy Covariance: A Practical Guide to Measurement and Data Analysis, 1st edn., Springer, Dordrecht, The Netherlands, 2012.

Baldocchi, D. D.: Assessing the eddy covariance technique for evaluating carbon dioxide exchange rates of ecosystems: past, present and future, Glob. Change Biol., 9, 479–492, 2003.

Beer, C., Reichstein, M., Tomelleri, E., Ciais, P., Jung, M., Carvalhais, N., Rödenbeck, C., Arain, M. A., Baldocchi, D., Bonan, G. B., Bondeau, A., Cescatti, A., Lasslop, G., Lindroth, A., Lomas, M., Luyssaert, S., Margolis, H., Oleson, K. W., Roupsard, O., Veenendaal, E., Viovy, N., Williams, C., Woodward, F. I., and Papale, D.: Terrestrial Gross Carbon Dioxide Uptake: Global Distribution and Covariation with Climate, Science, 329 (5993), 834–838, 2010.

Blackman, F. F.: Optima and limiting factors, Ann. Bot., 19, 281–296, 1905.

Bonan, G. B., Levis, S., Kergoat, L., and Oleson, K. W.: Landscapes as patches of plant functional types: an integrating concept for climate and ecosystem models, Global Biogeochem. Cy., 16, 5-1–5-23, 2002.

Cannell, M. G. R. and Thornley, J. H. M.: Temperature and CO_2 responses of leaf and canopy photosynthesis: a clarification using the non-rectangular hyperbola model of photosynthesis, Ann. Bot., 82, 883–892, 1998.

Davidson, E. A., Janssens, I. A., and Luo, Y.: On the variability of respiration in terrestrial ecosystems: moving beyond Q10, Glob. Change Biol., 12, 154–164, 2006.

Desai, A. R., Richardson, A. D., Moffat, A. M., Kattge, J., Hollinger, D. Y., Barr, A., Falge, E., Noormets, A., Papale, D., Reichstein, M., and Stauch, V. J.: Cross-site evaluation of eddy covariance GPP and RE decomposition techniques, Agric. Forest Meteorol., 148, 821–838, 2008.

Du, Z., Nie, Y., He, Y., Yu, G., Wang, H., and Zhou, X.: Complementarity of flux-and biometric-based data to constrain parameters in a terrestrial carbon model, Tellus B, 67, doi:10.3402/tellusb.v67.24102, 2015.

Foken, T., Göockede, M., Mauder, M., Mahrt, L., Amiro, B., and Munger, W.: Post-field data quality control, in: Handbook of Micrometeorology, edited by Lee, X., Massman, W., and Law, B., vol. 29

of Atmospheric and Oceanographic Sciences Library, Chap. 9, Springer, Dordrecht, The Netherlands, 181–208, 2005.

Gelman, A., Carlin, J. B., Stern, H. S., Dunson, D. B., Vehtari, A., and Rubin, D. B.: Bayesian Data Analysis, CRC Press, Boca Raton, 2013.

Gilmanov, T. G., Verma, S. B., Sims, P. L., Meyers, T. P., Bradford, J. A., Burba, G. G., and Suyker, A. E.: Gross primary production and light response parameters of four Southern Plains ecosystems estimated using long-term CO_2-flux tower measurements, Global Biogeochem. Cy., 17, 2, doi:10.1029/2002GB002023, 2003.

Gilmanov, T. G., Aires, L., Barcza, Z., Baron, V. S., Belelli, L., Beringer, J., Billesbach, D., Bonal, D., Bradford, J., Ceschia, E., Cook, D., Corradi, C., Frank, A., Gianelle, D., Gimeno, C., Gruenwald, T., Guo, H., Hanan, N., Haszpra, L., Heilman, J., Jacobs, A., Jones, M. B., Johnson, D. A., Kiely, G., Li, S., Magliulo, V., Moors, E., Nagy, Z., Nasyrov, M., Owensby, C., Pinter, K., Pio, C., Reichstein, M., Sanz, M. J., Scott, R., Soussana, J. F., Stoy, P. C., Svejcar, T., Tuba, Z., and Zhou, G.: Productivity, respiration, and light-response parameters of world grassland and agroecosystems derived from flux-tower measurements, Rangeland Ecol. Manag., 63, 16–39, 2010.

Gilmanov, T. G., Wylie, B. K., Tieszen, L. L., Meyers, T. P., Baron, V. S., Bernacchi, C. J., Billesbach, D. P., Burba, G. G., Fischer, M. L., Glenn, A. J., Hanan, N. P., Hatfield, J. L., Heuer, M. W., Hollinger, S. E., Howard, D. M., Matamala, R., Prueger, J. H., Tenuta, M., and Young, D. G.: CO_2 uptake and ecophysiological parameters of the grain crops of midcontinent North America: estimates from flux tower measurements, Agric. Ecosyst. Environ., 164, 162–175, 2013.

Goulden, M. L., Munger, J. W., Fan, S.-M., Daube, B. C., and Wofsy, S. C.: Measurements of carbon sequestration by long-term eddy covariance: methods and a critical evaluation of accuracy, Global Change Biol., 2(3), 169–182, 1996.

Hagen, S. C., Braswell, B. H., Linder, E., Frolking, S., Richardson, A. D., and Hollinger, D. Y.: Statistical uncertainty of eddy flux-based estimates of gross ecosystem carbon exchange at Howland Forest, Maine, J. Geophys. Res.-Atmos., 111, D08S03, doi:10.1029/2005JD006154, 2006.

Hamm, N. A. S., Atkinson, P. M., and Milton, E. J.: A per-pixel, non-stationary mixed model for empirical line atmospheric correction in remote sensing, Remote Sensing Environ., 124, 666–678, 2012.

Johnson, I. R.: PlantMod: exploring the physiology of plant canopies, IMJ Software, Melbourne, Australia, 2013.

Johnson, I. R., Thornley, J. H. M., Frantz, J. M., and Bugbee, B.: A model of canopy photosynthesis incorporating protein distribution through the canopy and its acclimation to light, temperature and CO_2, Ann. Bot., 106, 735–749, 2010.

Körner, C.: Leaf Diffusive Conductances in the Major Vegetation Types of the Globe, in: Ecophysiology of Photosynthesis, edited by: Schulze, E. D. and Caldwell, M. M., vol. 100 of Springer Study Edition, Chap. 22, Springer-Verlag, New York, 463–490, 1995.

Lasslop, G., Reichstein, M., Papale, D., Richardson, A. D., Arneth, A., Barr, A., Stoy, P., and Wohlfahrt, G.: Separation of net ecosystem exchange into assimilation and respiration using a light response curve approach: critical issues and global evaluation, Glob. Change Biol., 16, 187–208, 2010.

Lewis, J. D., McKane, R. B., Tingey, D. T., and Beedlow, P. A.: Vertical gradients in photosynthetic light response within an old-growth Douglas-fir and western hemlock canopy, Tree Physiol., 20, 447–456, 2000.

Li, X., Liang, S., Yu, G., Yuan, W., Cheng, X., Xia, J., Zhao, T., Feng, J., Ma, Z., Ma, M., Liu, S., Chen, J., Shao, C., Li, S., Zhang, X., Zhang, Z., Chen, S., Ohta, T., Varlagin, A., Miyata, A., Takagi, K., Saiqusa, N., and Kato, T.: Estimation of gross primary production over the terrestrial ecosystems in China, Ecol. Model., 261/262, 80–92, 2013.

Long, S. P., Zhu, X.-G., Naidu, S. L., and Ort, D. R.: Can improvement in photosynthesis increase crop yields?, Plant Cell Environ., 29, 315–330, 2006.

Lunn, D., Thomas, A., Best, N., and Spiegelhalter, D.: WinBUGS – a Bayesian modelling framework: Concepts, structure, and extensibility, Stat. Comput., 10, 325–337, 2000.

Lunn, D., Jackson, C., Best, N., Thomas, A., and Spiegelhalter, D.: The BUGS Book – A Practical Introduction to Bayesian Analysis, CRC Press, Boca Raton, 2013.

Mahecha, M. D., Reichstein, M., Carvalhais, N., Lasslop, G., Lange, H., Seneviratne, S. I., Vargas, R., Ammann, C., Arain, M. A., Cescatti, A., Janssens, I. A., Migliavacca, M., Montagnani, L., and Richardson, A. D.: Global convergence in the temperature sensitivity of respiration at ecosystem level, Science, 329, 838–840, 2010.

Minet, J., Laloy, E., Tychon, B., and François, L.: Bayesian inversions of a dynamic vegetation model at four European grassland sites, Biogeosciences, 12, 2809–2829, doi:10.5194/bg-12-2809-2015, 2015.

Mohren, G. M. J.: Simulation of forest growth, applied to Douglas fir stands in the Netherlands, Ph.D. thesis, Wageningen Agriculture university, The Netherlands, 1987.

Monteith, J. L. and Unsworth, M. H.: Principles of Environmental Physics, Edward Arnold, Sevenoaks, UK, 2nd edn., 1990.

Moncrieff, J. B., Malhi, Y., Leuning, R.: The propagation of errors in long-term measurements of land-atmosphere fluxes of carbon and water. Glob. Change Biol. 2 (3), 231–240, 1996.

Oakley, J. E. and O'Hagan, A.: Uncertainty in prior elicitations: a nonparametric approach, Biometrika, 94, 427–441, 2007.

Ogren, E.: Convexity of the photosynthetic light-response curve in relation to intensity and direction of light during growth, Plant Physiol., 101, 1013–1019, 1993.

Raj, R., Hamm, N. A. S., van der Tol, C., and Stein, A.: Variance-based sensitivity analysis of BIOME-BGC for gross and net primary production, Ecol. Model., 292, 26–36, 2014.

Rabinowitch, E. I: Photosynthesis and Related Processes, Soil Science, 72, 482, 1951.

Reichstein, M., Falge, E., Baldocchi, D., Papale, D., Aubinet, M., Berbigier, P., Bernhofer, C., Buchmann, N., Gilmanov, T., Granier, A., Grünwald, T., Havránková, K., Ilvesniemi, H., Janous, D., Knohl, A., Laurila, T., Lohila, A., Loustau, D., Matteucci, G., Meyers, T., Miglietta, F., Ourcival, J.-M., Pumpanen, J., Rambal, S., Rotenberg, E., Sanz, M., Tenhunen, J., Seufert, G., Vaccari, F., Vesala, T., Yakir, D., and Valentini, R.: On the separation of net ecosystem exchange into assimilation and ecosystem respiration: review and improved algorithm, Glob. Change Biol., 11, 1424–1439, 2005.

Ricciuto, D. M., Davis, K. J., and Keller, K.: A Bayesian calibration of a simple carbon cycle model: The role of observations in estimating and reducing uncertainty, Global Biogeochem. Cy., 22, 2, doi:10.1029/2006GB002908, 2008.

Richardson, A. D. and Hollinger, D. Y.: Statistical modeling of ecosystem respiration using eddy covariance data: Maximum likelihood parameter estimation, and Monte Carlo simulation of model and parameter uncertainty, applied to three simple models, Agric. Forest Meteorol., 131, 191–208, 2005.

Richardson, A. D., Braswell, B. H., Hollinger, D. Y., Burman, P., Davidson, E. A., Evans, R. S., Flanagan, L. B., Munger, J. W., Savage, K., Urbanski, S. P., and Wofsy, S. C.: Comparing simple respiration models for eddy flux and dynamic chamber data, Agric. Forest Meteorol., 141, 219–234, 2006a.

Richardson, A. D., Hollinger, D. Y., Burba, G. G., Davis, K. J., Flanagan, L. B., Katul, G. G., Munger, J. W., Ricciuto, D. M., Stoy, P. C., Suyker, A. E., Verma, S. B., Wofsy, S. C.: A multi-site analysis of random error in tower-based measurements of carbon and energy fluxes. Agric. Forest Meteorol., 136, 1–18, 2006b.

Richardson, A. D., Mahecha, M. D., Falge, E., Kattge, J., Moffat, A. M., Papale, D., Reichstein, M., Stauch, V. J., Braswell, B. H., Churkina, G., Kruijt, B., Hollinger, D. Y.: Statistical properties of random CO_2 flux measurement uncertainty inferred from model residuals. Agric. Forest Meteorol., 148 , 38–50, 2008.

Ripullone, F., Grassi, G., Lauteri, M., and Borghetti, M.: Photosynthesis–nitrogen relationships: interpretation of different patterns between *Pseudotsuga menziesii* and *Populus x euroamericana* in a mini-stand experiment, Tree Physiol., 23, 137–144, 2003.

Ruimy, A., Jarvis, P., Baldocchi, D., and Saugier, B.: CO_2 fluxes over plant canopies and solar radiation: a review, Adv. Ecol. Res., 26, 1–68, 1995.

Running, S. W., Nemani, R. R., Heinsch, F. A., Zhao, M., Reeves, M., and Hashimoto, H.: A continuous satellite-derived measure of global terrestrial primary production, BioScience, 54, 547–560, 2004.

Skillman, J. B.: Quantum yield variation across the three pathways of photosynthesis: not yet out of the dark, J. Exp. Bot., 59, 1647–1661, 2008.

Steingrover, E. G. and Jans, W. W. P.: Physiology of forest-grown Douglas fir trees: Effect of air pollution and drought, Tech. Rep. 94/3, IBN DLO, Institute for Forestry and Nature Research, Wageningen, the Netherlands, 1994.

Stoy, P. C., Katul, G. G., Siqueira, M. B. S., Juang, J.-Y., Novick, K. A., Uebelherr, J. M., and Oren, R.: An evaluation of models for partitioning eddy covariance-measured net ecosystem exchange into photosynthesis and respiration, Agric. Forest Meteorol., 141, 2–18, 2006.

Su, Z., Timmermans, W. J., van der Tol, C., Dost, R., Bianchi, R., Gómez, J. A., House, A., Hajnsek, I., Menenti, M., Magliulo, V., Esposito, M., Haarbrink, R., Bosveld, F., Rothe, R., Baltink, H. K., Vekerdy, Z., Sobrino, J. A., Timmermans, J., van Laake, P., Salama, S., van der Kwast, H., Claassen, E., Stolk, A., Jia, L., Moors, E., Hartogensis, O., and Gillespie, A.: EAGLE 2006 – Multi-purpose, multi-angle and multi-sensor in-situ and airborne campaigns over grassland and forest, Hydrol. Earth Syst. Sci., 13, 833–845, doi:10.5194/hess-13-833-2009, 2009.

Sun, J., Guan, D., Wu, J., Jing, Y., Yuan, F., Wang, A., and Jin, C.: Day and night respiration of three tree species in a temperate forest of northeastern China, iForest - Biogeosciences and Forestry, 8 (1), 25-32, 2015.

Teskey, R.O., Saveyn, A., Steppe, K., and McGuire, M.A.: Origin, fate and significance of CO_2 in tree stems, New Phytol., 177 (1), 17-32, 2008.

Thornley, J. H. M.: Instantaneous canopy photosynthesis: analytical expressions for sun and shade leaves based on exponential light decay down the canopy and an acclimated non-rectangular hyperbola for leaf photosynthesis, Ann. Bot., 89, 451–458, 2002.

Thornley, J. H. M. and Johnson, I. R.: Plant and crop modelling, in: A Mathematical approach to Plant and Crop Physiology, The Blackburn Press, Caldwell, New Jersey, 2000.

Thornton, P. E.: Description of a numerical simulation model for predicting the dynamics of energy, water, carbon, and nitrogen in a terrestrial ecosystem, Ph.D. thesis, University of Montana, Missoula, 1998.

van der Tol, C., Verhoef, W., Timmermans, J., Verhoef, A., and Su, Z.: An integrated model of soil-canopy spectral radiances, photosynthesis, fluorescence, temperature and energy balance, Biogeosciences, 6, 3109–3129, doi:10.5194/bg-6-3109-2009, 2009.

van Wijk, M. T., Dekker, S. C., Bouten, W., Bosveld, F. C., Kohsiek, W., Kramer, K., and Mohren, G. M. J.: Modeling daily gas exchange of a Douglas-fir forest: comparison of three stomatal conductance models with and without a soil water stress function, Tree Physiol., 20, 115–122, 2000.

van Wijk, M. T., Dekker, S. C., Bouten, W., Kohsiek, W., and Mohren, G. M. J.: Simulation of carbon and water budgets of a Douglas-fir forest, Forest Ecology and Management, 145, 229–241, 2001.

van Wijk, M. T., Bouten, W., and Verstraten, J. M.: Comparison of different modelling strategies for simulating gas exchange of a Douglas-fir forest, Ecol. Model., 158, 63–81, 2002.

Wang, H., Jia, G., Fu, C., Feng, J., Zhao, T., and Ma, Z.: Deriving maximal light use efficiency from coordinated flux measurements and satellite data for regional gross primary production modeling, Remote Sensing Environ., 114, 2248–2258, 2010.

Warren, C. R., Ethier, G. J., Livingston, N. J., Grant, N. J., Turpin, D. H., Harrison, D. L., and Black, T. A.: Transfer conductance in second growth Douglas-fir (*Pseudotsuga menziesii* (Mirb.)Franco) canopies, Plant Cell Environ., 26, 1215–1227, 2003.

Table 1. List of symbols with unit.

NEE, **y**	net ecosystem exchange	mg $CO_2\,m^{-2}\,s^{-1}$
P_a	gross CO_2 assimilation	mg $CO_2\,m^{-2}\,s^{-1}$
GPP	gross primary production	mg C $m^{-2}\,s^{-1}$; g C $m^{-2}\,d^{-1}$
R_{eco}	ecosystem respiration	mg $CO_2\,m^{-2}\,s^{-1}$
PPFD	photosynthetic photon flux density	µmol quanta $m^{-2}\,s^{-1}$
T_a	air temperature	°C
α	quantum yield	mg CO_2 (µmol quanta)$^{-1}$
θ	degree of curvature of light response curve	unitless
A_{max}	photosynthetic capacity at light saturation	mg $CO_2\,m^{-2}\,s^{-1}$
k_T	temperature sensitive parameter	(°C)$^{-1}$
r_0	ecosystem respiration at reference temperature T_a = 0 °C	mg $CO_2\,m^{-2}\,s^{-1}$
τ_e	precision of the normal distribution of the likelihood	
$\boldsymbol{\beta}$	(θ, α, A_{max}, r_0, k_T)	
R_b	ecosystem respiration at reference temperature T_a = 15 °C	g $CO_2\,m^{-2}\,s^{-1}$
Q_{10}	multiplication factor to respiration with 10 °C increase in T_a	
RH	relative humidity	%
VPD	vapour pressure deficit	kPa
VPD_{cr}	critical value of vapour pressure deficit	kPa
ϕ	vapour pressure deficit response function	
σ_{VPD}	curvature parameter for ϕ	kPa

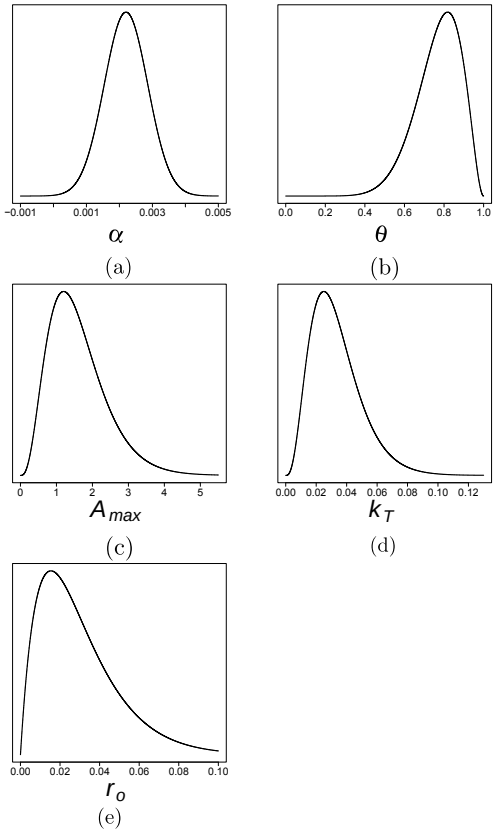

Figure 1. Informative prior distribution of the NRH model parameters: **(a)** $\alpha \sim N(\mu_\alpha = 0.0022, \sigma_\alpha = 0.00066)$, **(b)** $\theta \sim \text{Beta}(\text{shape1} = 10, \text{shape2} = 3)$, **(c)** $A_{\text{max}} \sim \text{Gamma}(\text{shape} = 4, \text{rate} = 2.5)$, **(d)** $k_{\text{T}} \sim \text{Gamma}(\text{shape} = 4, \text{rate} = 120)$, **(e)** $r_0 \sim \text{Beta}(\text{shape1} = 2, \text{shape2} = 64)$. Information about the NRH parameters is given in Table 1. The y axis represents the density of corresponding distribution.

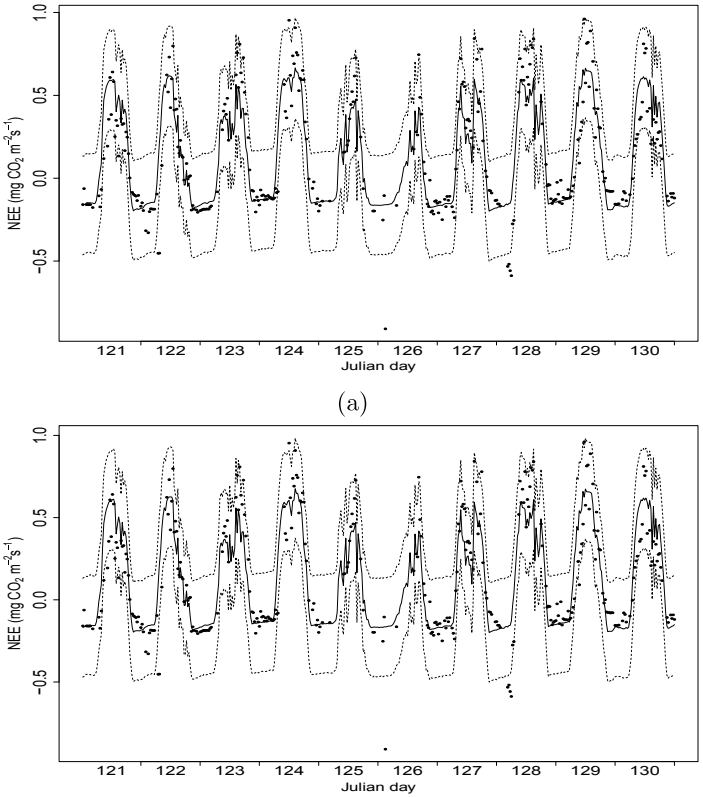

Figure 2. Median (solid lines) and 95 % credible intervals (dashed lines) of the posterior distribution of NEE together with half-hourly NEE measurements (solid points) for a 10-day block (1 May to 10 May 2009, Julian days 121 to 130): **(a)** when using informative prior distributions, **(b)** when using non-informative prior distributions.

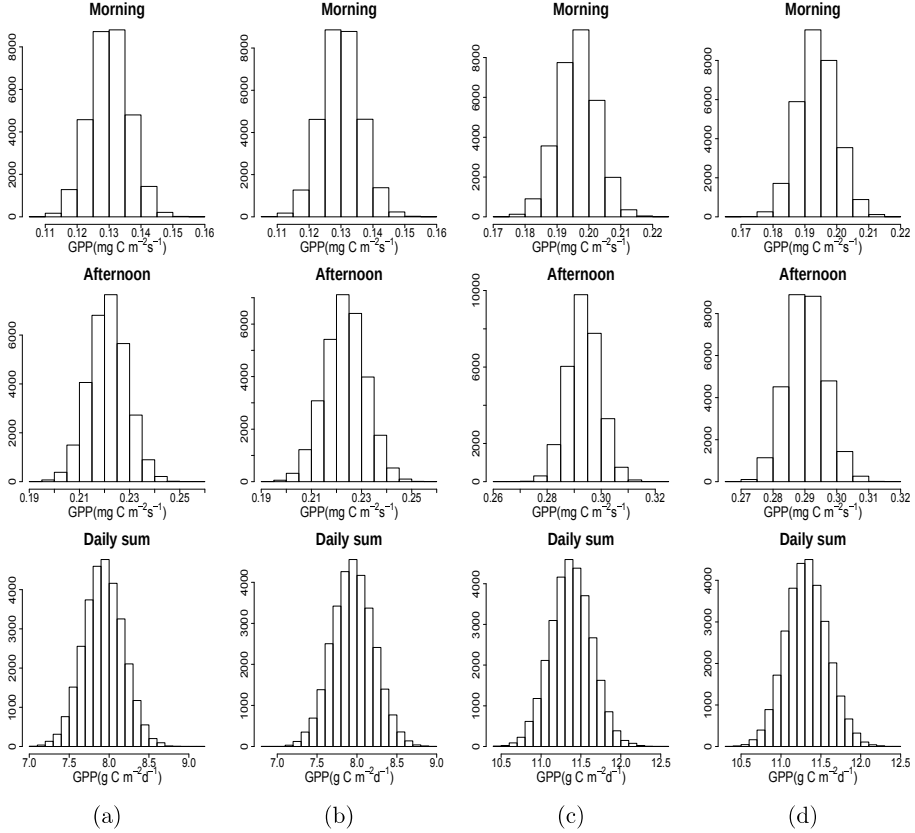

Figure 3. Histograms of half hourly GPP (Morning and afternoon) and daily sum of GPP when using: **(a)** informative priors on Julian day 121 (1 May 2009), **(b)** non-informative priors on Julian day 121, **(c)** informative priors on Julian day 196 (15 July 2009), **(d)** non-informative priors on Julian day 196. The morning and afternoon time belong to half-hour 8:00 CET to 8:30 CET and 13:00 CET to 13:30 CET respectively. The y axis is frequency; CET is Central European Time.

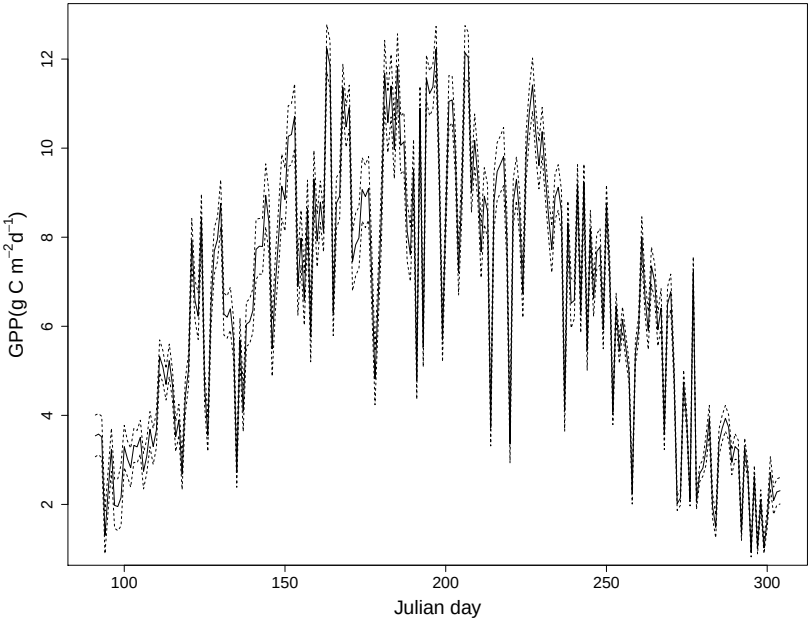

Figure 4. Median (solida line) and 95% credible intervals (dashed lines) of daily GPP distributions during the growing season of 2009 (1st April to 31st October 2009, Julian days 91 to 304) for the choice of informative prior distributions.

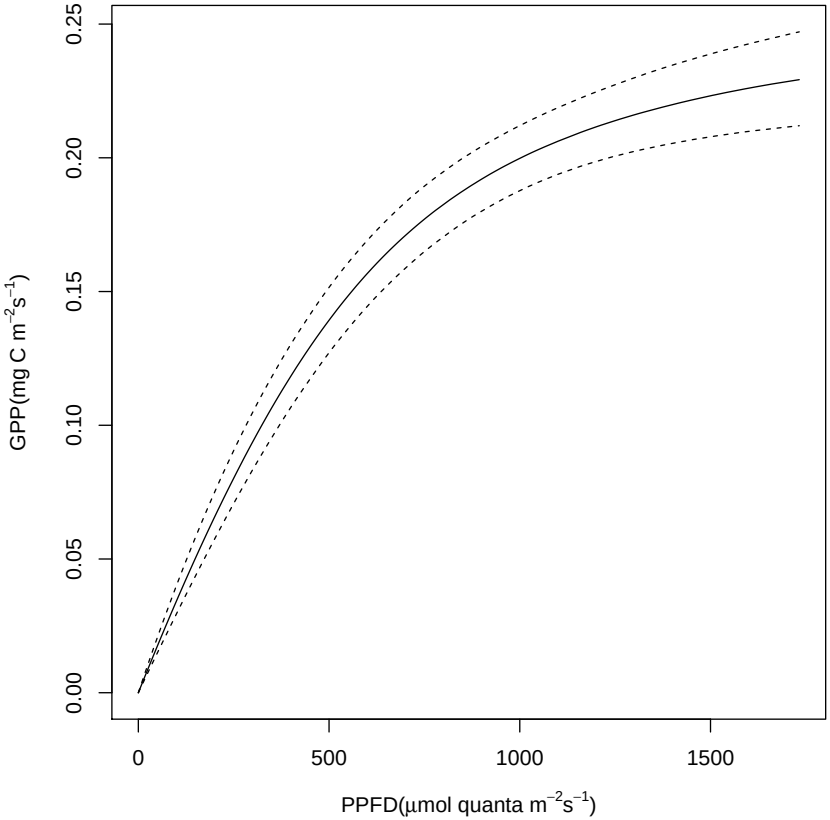

Figure 5. Median (solid line) and 95 % credible intervals (dashed lines) of half-hourly gross primary production (GPP) with photosynthetic photon flux density (PPFD) for a 10-day block (1 May to 10 May 2009, Julian days 121 to 130) for the choice of informative prior distributions.

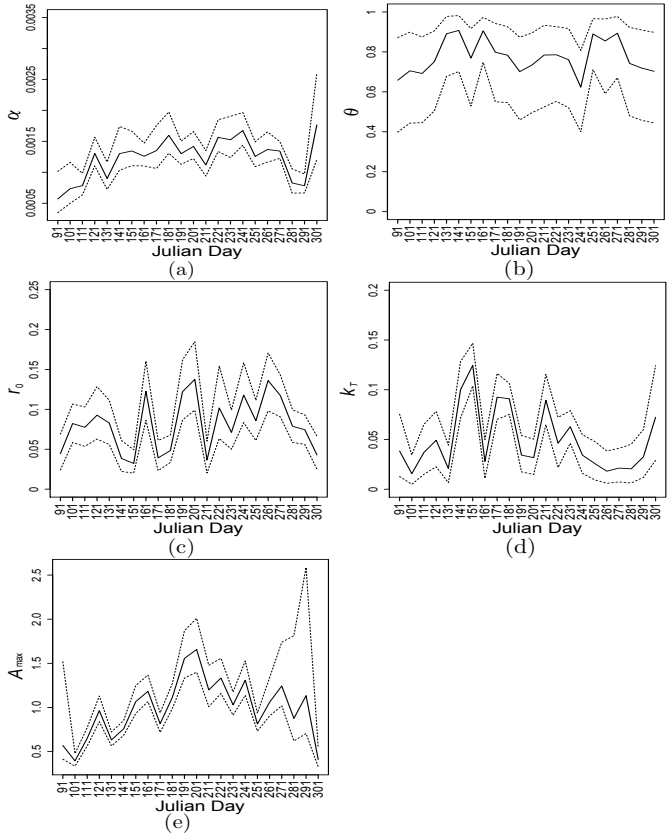

Figure 6. Median (solid lines) and 95 % credible intervals (dashed lines) of the posterior distributions of the NRH parameters when using informative prior distributions for each 10-day block during the growing season in 2009. The x axis is the first Julian day of each 10-day block. The y axis represents NRH parameter. Information about the NRH parameters is given in Table 1.

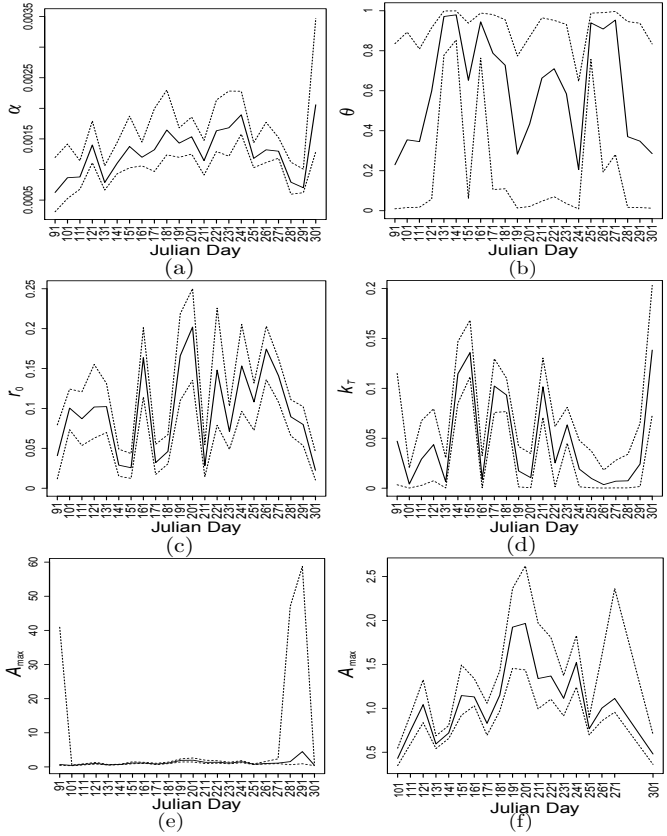

Figure 7. As Fig. 6 when using non-informative prior distributions. To help visualization of $A_{\max}$ we have added a subfigure **(f)** with the spikes removed (i.e., without the blocks of Julian days 91–100, 281–290, and 291–300).

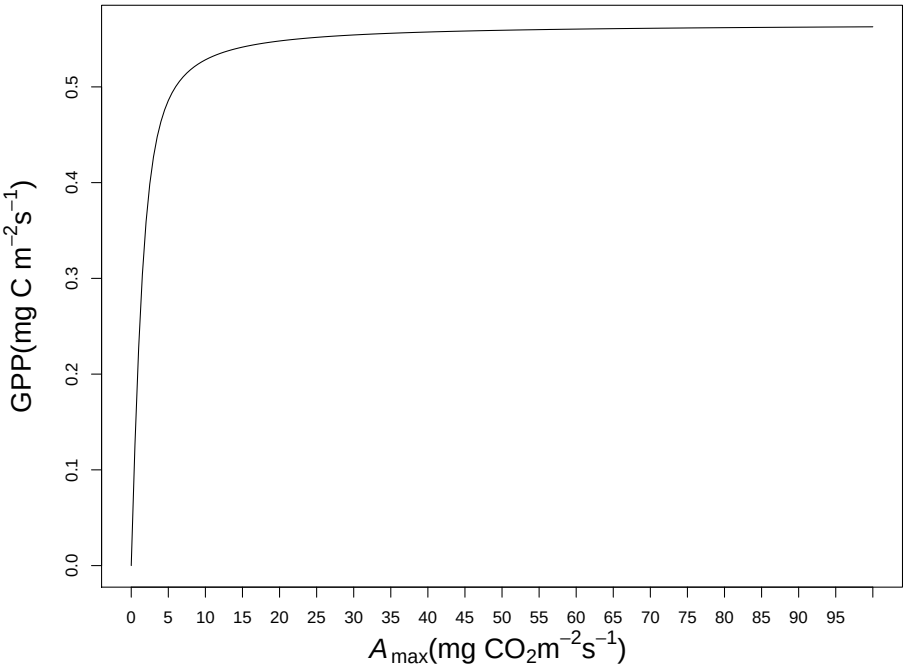

Figure 8. Variation of gross primary production (GPP) with the variation of photosynthetic capacity (A_{max}) from 0 to 100 mg CO_2 m^{-2} s^{-1}. The values of quantum yield (α), degree of curvature (θ), ecosystem respiration at reference temperature (r_0), and temperature sensitive paramete (k_{T}) are fixed at 0.7, 0.0022, 0.1, 0.07 respectively. Air temperature (T_{a}) and photosynthetic photon flux density (PPFD) are fixed at 10 °C and 900 µmol quanta m^{-2} s^{-1}.